CHEMISTRY OF MATERIALS
Cite This: Chem. Mater. XXXX, XXX, XXX−XXX
Article
pubs.acs.org/cm

Interfacial Drawing: Roll-to-Roll Coating of Semiconducting Polymer and Barrier Films onto Plastic Foils and Textiles

Rory Runser,[†] Samuel E. Root,[†] Derick E. Ober, Kartik Choudhary, Alex X. Chen, Charles Dhong, Armando D. Urbina, and Darren J. Lipomi*

Department of NanoEngineering, University of California San Diego, 9500 Gilman Drive, Mail Code 0448, La Jolla, California 92093-0448, United States

Supporting Information

ABSTRACT: This paper demonstrates that a thin polymeric film (10−80 nm) can be continuously drawn from the meniscus of a nonpolar polymer solution at an air−water−fluoropolymer interface using a roll-to-roll process: "interfacial drawing". With this process, it is possible to control the thickness of the film by manipulating the concentration of the solution, along with the drawing velocity of the receiving substrate. We demonstrate the formation of thin films >1 m in length and 1000 cm^2 in area, using our custom-designed apparatus. Interfacial drawing has three characteristics which compare favorably to other methods of forming and depositing polymeric thin films. First, the films are solidified prior to deposition, which means that they can be used to uniformly coat nonplanar, rough, or porous substrates. Second, these films can be stacked into multilayered architectures without risk of redissolving the layer beneath. Third, for some materials, the process yields films with superior mechanical compliance for applications such as wearable or flexible devices, compared to films produced by spin-coating. We demonstrate the utility of interfacial drawing by forming thin films of various semiconducting polymers, including the active layers of all-polymer bulk heterojunction solar cells as well as barrier coatings. As part of these demonstrations, we show how floating polymeric films can be transferred easily to diverse substrates, including those with rough and irregular surfaces, such as textiles and fabrics.

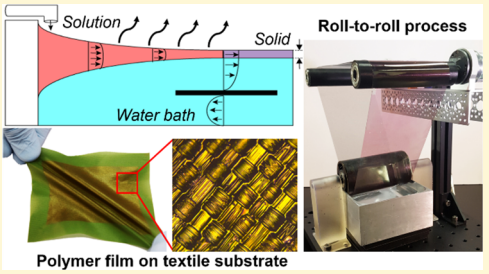

1. INTRODUCTION

Thin films of polymers are required for a myriad of technological applications, ranging from simple protective coatings to advanced multilayer laminates for flexible electronic devices. A major challenge associated with existing roll-to-roll (R2R) processes for manufacturing multilayer laminates of polymers is the redissolution of layers during iterative steps of deposition from solution. Some methods of addressing this challenge include transfer printing,[1−3] vacuum deposition,[4,5] and casting layers from orthogonal solvents.[6,7] While these approaches are useful for designing lab-scale devices, in most large-scale, R2R processes for thin-film deposition, such as slot-die coating, blade coating, and screen printing, the material of interest does not solidify until after it is deposited onto the substrate.[8] Here, we introduce an R2R-compatible process, "interfacial drawing", in which a solid polymer film is drawn onto a substrate directly from a liquid meniscus at an air−water−fluoropolymer interface (Figure 1).

The transport processes underlying interfacial drawing are based on the phenomenon of surface tension-driven flow of organic media on water. The first investigations into interfacial spreading have been attributed to Benjamin Franklin who, in 1773, discovered that a spoonful of oil deposited onto a pond would spread out over a very large area, evidenced by the quelling of surface waves underneath.[9] A century later, Lord Rayleigh quantified this observation by determining the thickness of the resulting oil monolayer.[10] Further advances by Agnes Pockels,[11] and later, Irving Langmuir and Katherine Blodgett, led to the development of the Langmuir−Blodgett (LB) trough,[12] which enabled scientists to deposit a monolayer film of organic materials onto a solid support. These advances paved the way for improved optical coatings, transparent glass, and nanoparticle thin films.[13−17]

While much of the early research into LB films involved coatings made from amphiphilic small molecules, such as fatty acids, more recent work has investigated the processing of polymer solutions. The spreading of a polymer solution is dictated by the solution viscosity, volatility, and interfacial surface tension between the supporting liquid (typically water) and the organic solvent[18] (Figure S1a). This process can yield ultrathin (∼10−80 nm) polymeric films, which have a variety of applications.[19−21] For example, a recent work by Noh et al. has applied this method to fabricate semiconducting polymer films, and has shown that the process could yield organic solar cells with improved efficiencies compared to devices fabricated by spin-coating.[22] The spontaneous nature of the solvent spreading on water also enables the generation of large-area polymeric thin films.[23] This observation motivated us to

Received: August 19, 2019
Revised: October 1, 2019
Published: October 2, 2019

DOI: 10.1021/acs.chemmater.9b03343
Chem. Mater. XXXX, XXX, XXX−XXX

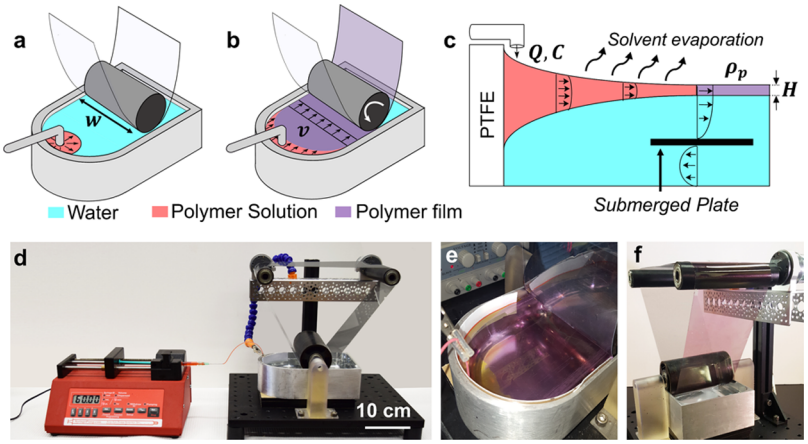

Figure 1. Schematic drawings and photographs of the interfacial drawing process. (a) Start-up, (b) continuous operation, and (c) cross-sectional view (not to scale) of the process. All variables are defined in Table 1. (d) Photograph of the benchtop apparatus, including a syringe pump to control the flow of polymer solution. (e) Top-down view of polymer film on top of water bath. (f) Backside view showing polymer film coated onto a flexible polyethylene terephthalate (PET) substrate.

convert this batch process into a continuous, roll-to-roll (R2R) process, which would enable the formation of much larger films at a faster rate.[24] The resulting process can generate polymer films of >1 m in length, with our benchtop setup.

Interfacial drawing provides an opportunity for producing large-area multilayer polymer thin films processed from the same (or similar) solvents, which could enable the fabrication of new architectures for OLEDs,[25] organic solar cells,[26] and reflective birefringent optics.[27] Additionally, the ability of interfacial drawing to coat uniform, ultrathin (10−20 nm) polymer films (which is often difficult to achieve with other coating techniques[8]) would be beneficial to a number of fields, including sensors,[17] antireflection coatings,[12] and biomedical devices.[28] The ability to observe the film quality prior to deposition to the desired substrate would also be advantageous for quality control purposes in a manufacturing setting. Furthermore, interfacial drawing allows for the use of unusual and irregular substrates, as a presolidified film can be adhered onto the surface, rather than drying nonuniformly in pores and gaps. This capability could be of interest for developing conductive fabrics,[29−33] wearable optoelectronic devices,[34−36] or textiles with barrier coatings. In this report, we investigate in detail the operating principles behind interfacial drawing and characterize the mechanical and optoelectronic properties of the resulting films.

2. PROCESS DESIGN

2.1. Design of Benchtop Apparatus. Interfacial drawing generates a uniform polymer thin film by leveraging the spontaneous spreading and drying process of a polymer solution deposited at an air−water−fluoropolymer interface (Figure 1a). When the solidified edge of the film is drawn onto a flexible or textile substrate, the liquid meniscus continues to spread and solidify in a continuous process (Figure 1b,c). Photographs of our custom-designed benchtop apparatus are shown in Figure 1d−f. More detailed, annotated images and movies of the setup and operation are found in the Supporting Information (Figure S2a and Movies S1 and S2). Briefly, we custom-milled a 10 cm-wide trough in an aluminum block to serve as the water bath. (We previously found that a 3D-printed, plastic trough absorbed the solvent and became difficult to clean between trials.) A trough having a semicircular edge on the end where the solution was injected was found to be preferable to a rectangular trough, as the curvature eliminated corners which became sites where the polymer film would tear. We placed a strip of adhesive-coated poly(tetrafluoroethylene) (PTFE) along the curved edge to encourage the formation of a polymer solution meniscus at the PTFE−water interface. A thin plate was submerged in the center of the trough to promote a circulatory flow within the water bath, which helped reduce eddies and variations in velocity on the surface of the water bath. The roll-to-roll mechanism was constructed with 3D-printed rollers, which supported a ∼0.5 m loop of flexible poly(ethylene terephthalate) (PET). The rollers were operated by DC gear motors, which were connected to a power supply with a variable voltage output, to control the drawing velocity (Figure S2b). The apparatus was partially shielded from external sources of vibration by supporting it on a platform with dampening rubber feet. Fumes from the chlorinated solvents were suctioned from above the process using a maneuverable exhaust snorkel.

2.2. Choice of Polymer Solution. *2.2.1. Choice of Solvent.* While interfacial drawing is theoretically compatible with any polymer−solvent system with a positive spreading parameter (Figure S1a), we limited our studies to solutions prepared in chlorobenzene, a common solvent for dissolving polymeric materials, which also has a favorable spreading parameter. Other solvents, which were considered but not used, are listed in Tables S3 and S4.

2.2.2. Choice of Polymers. Interfacial drawing is best suited for mechanically robust polymers, which are resistant to tearing during the drawing process. For this study, semiconducting polymers were chosen as a model system because (i) their applications are exclusively limited to thin-film geometries, (ii) they exhibit a wide range of mechanical properties,[37] and (iii) they strongly absorb visible light; thus, they exhibit an abrupt color change upon solidification,[38] and film thickness can be linearly correlated to UV−vis absorption for rapid optical measurement of thickness on flexible substrates. Nevertheless, this process is not limited to optically active polymers, and we also successfully fabricated films of conventional transparent plastics.

DOI: 10.1021/acs.chemmater.9b03343
Chem. Mater. XXXX, XXX, XXX−XXX

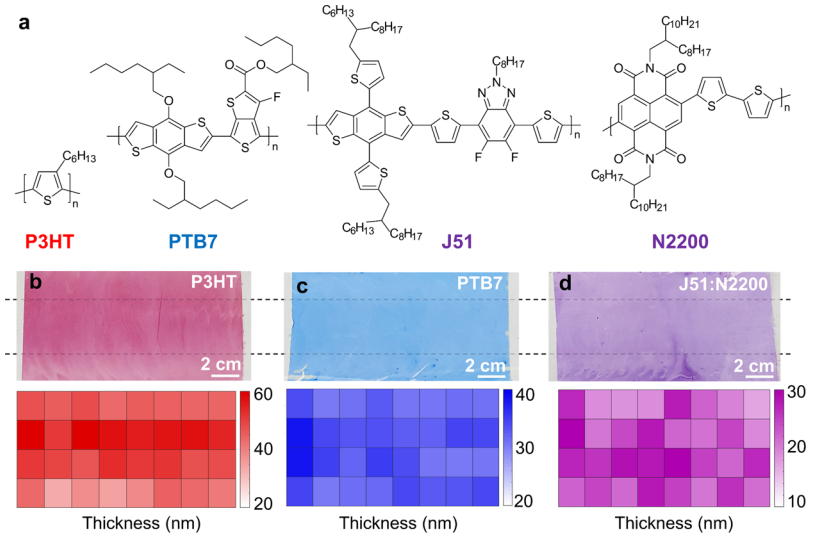

Figure 2. Semiconducting polymer films produced by interfacial drawing: chemical structures, photographs, and thickness maps. (a) Chemical structures of polymers used. Refer to Materials and Methods section for systematic names. (b–d) Films with dimensions of 10 cm × 20 cm produced using interfacial drawing and corresponding thickness maps obtained from UV–vis absorption intensity, indicating the variation in thickness for (b) P3HT, (c) PTB7, and (d) J51:N2200. Each square in the heatmaps corresponds to an area of 2.5 cm × 2.5 cm. The central region of the films (denoted by the dashed lines) was found to be of a more uniform thickness than the outside edges. For these films, Q = 40 μL min^{-1}, v = 3 mm s^{-1}, and C = 20 mg mL^{-1} for P3HT and PTB7, and C = 12 mg mL^{-1} for J51:N2200.

The structures of the materials used in this study are given in Figure 2a. To investigate the utility of interfacial drawing for materials with various microstructures and mechanical properties, we began our study using PTB7, a predominantly amorphous polymer,[39] and P3HT, a semicrystalline polymer, which is often considered a model material in semiconducting polymer research.[40] Large-area (10 cm × 20 cm) thin films of these materials made using interfacial drawing and coated onto a flexible PET substrate are shown in Figure 2b,c. We did note some tears and variations in thickness within the outer 2 cm edges of these films, likely due to uneven circulation of the water along the edges of the trough. The middle regions of the films (indicated by the dashed lines in Figure 2b–d), however, were uniform, with variations of ±3–6 nm from the average. Additionally, we sometimes observed wrinkling in P3HT films, likely due to the glassy nature of P3HT at room temperature (in contrast to PTB7, which did not exhibit wrinkling). The addition of a plasticizer, such as 1,8-diiodooctane (DIO; often used as an additive to improve the performance of organic solar cells), served to eliminate these wrinkles from P3HT films (Figure S4a,b).

To demonstrate the utility of interfacial drawing for the fabrication of functional organic electronic devices, we selected a binary mixture of two polymers, J51:N2200 (Figure 2d). All-polymer blends often possess improved mechanical resilience compared to polymer:fullerene blends,[41] and this particular blend has previously been shown to yield high-efficiency solar cells.[42] We also attempted to combine P3HT and PTB7 with the methonofullerene $PC_{61}BM$ to make a bulk heterojunction organic solar cell.[43] However, these blends yielded films that cracked upon solidification (Figure S3g,h), which was not surprising given the embrittling effect of fullerenes.[37]

3. RESULTS AND DISCUSSION

3.1. Characterization of Process Variables. *3.1.1. Relevant Process Variables.* When a polymer solution is initially injected at the water–air–PTFE interface at the pump rate, Q, it spreads in two directions: (i) circumferentially to form a liquid meniscus along the semicircular interface and (ii) onto the surface of the water to form a thin liquid film, which dries rapidly and solidifies (see Movie S1). In theory, the characteristic thickness, H, of the dried film depends upon the surface tension, viscosity, and mass transfer coefficient of the polymer solution, all of which, in turn, depend upon the polymer–solvent system employed and the initial concentration of the polymer, C. When the solidified edge of the film is drawn by the roller onto the substrate at a linear velocity, v, liquid from the meniscus spreads and dries to replenish the solid film with a resulting thickness that should be inversely dependent upon velocity at which it is drawn. A series of pilot experiments showed that, for a trough with width, w = 10 cm, the process operated viably for $Q \approx 10$ μL min^{-1}, $v \approx 1$ mm s^{-1}, and $C \approx 10$ mg mL^{-1} and that variations in the concentration of the polymer solution resulted in the most pronounced changes in film thickness.

3.1.2. Effect of Polymer Concentration. To assess the range of film thickness attainable by modulating the initial polymer concentration, we chose a fixed Q of 40 μL min^{-1} and v of 3 mm s^{-1} and ran a set of trials in which the concentration was incrementally increased from 5 to 40 mg mL^{-1}. As shown in Figure 3a,b, we observed a linear correlation between film thickness and concentration of polymer for all three polymer solutions tested. Given similarities in surface tension, viscosity, and evaporative mass transfer coefficient of these three chlorobenzene–polymer solutions, it is not surprising that they all exhibited similar slopes relating concentration to thickness. For the solutions tested, the minimum thickness attainable was between 5 and 10 nm for a concentration of 5 mg mL^{-1}. Below this concentration, the films did not exhibit sufficient mechanical robustness to be pulled by the roller without tearing. The maximum thickness attainable ranged from 30 nm for the J51:N2200 blend to 80 nm for P3HT. The P3HT solution was capable of spreading reliably up to a viscosity of 10 MPa s at 40 mg mL^{-1} (see Table S5 for

DOI: 10.1021/acs.chemmater.9b03343
Chem. Mater. XXXX, XXX, XXX–XXX

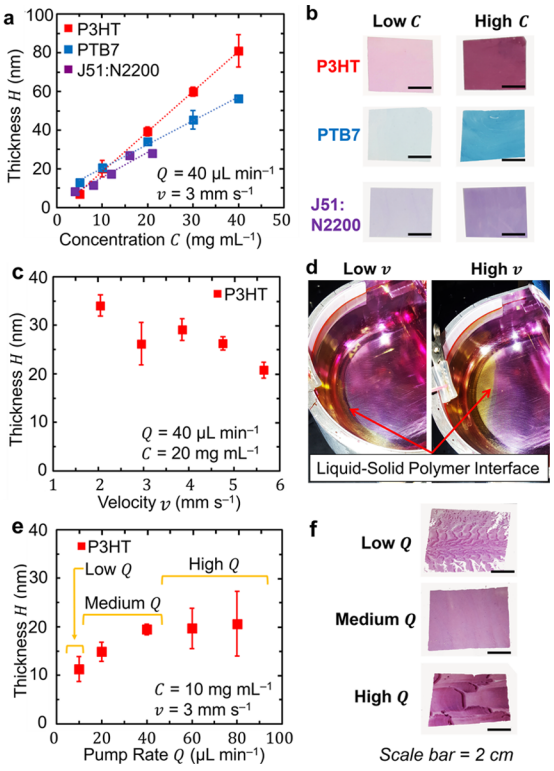

Figure 3. Process characterization. (a) Plot showing the dependence of thickness on solution concentration. (b) Photos of samples made from low and high concentrations. (c) Plot showing dependence of thickness on drawing velocity. (d) Top-down photograph process showing the effect of drawing velocity on the boundary between the liquid solution (orange) and solid polymer (purple). (e) Plot showing dependence of thickness on pump rate. (f) Photos of samples made from three regimes of pump rates.

viscosity data), while the J51:N2200 blend exhibited non-Newtonian gel-like behavior, which prevented reliable spreading at the same concentration.

3.1.3. Effect of Drawing Velocity. The maximum rate for producing a film by interfacial drawing is limited by the linear velocity of the roller. To investigate the effect of this critical manufacturing parameter, we selected the mid-range concentration of P3HT (20 mg mL^{-1}), fixed the flowrate at 40 μL min^{-1}, and incrementally varied the drawing velocity from 2 to 6 mm s^{-1}. As shown in Figure 3c, we observed that the thickness decreased as the film was drawn at a faster rate. Moreover, we observed that increasing v caused the liquid–solid polymer interface on the water bath surface to be pulled further away from the wall (Figure 3d). Importantly, the system remained operable until the liquid–solid boundary came in contact with the roller, suggesting that interfacial drawing could be scaled up to a larger system with faster operating speeds if it were designed with the appropriate water bath geometry (i.e., sufficient distance between the meniscus and the substrate rollers).

3.1.4. Effect of Pump Rate. The final parameter that was varied in our initial characterization of the system was the volumetric pump rate of polymer solution, Q (Figure 3e,f). We observed three regimes of film solidification behavior: At low values of Q (<5 μL min^{-1}), there was extensive film tearing due to an insufficient quantity polymer solution being supplied to the system; for high values of Q (>40 μL min^{-1}), films exhibited uneven solidification patterns; in the intermediate regime, we observed uniform films with H being proportional to Q. It can be expected that the intermediate regime of Q corresponds to steady-state conditions.

3.1.5. Steady-State Analysis. A mass balance applied to the solid polymer in the process yields the following relation

$$C\frac{dV_m}{dt} = \left[\frac{10^{-3}\ \text{mL}}{\mu\text{L}}\right]QC - \left[\frac{6\times10^{-4}\ \text{s·mg·cm}^2}{\text{min·g·nm·mm}}\right]v\rho_p wH \quad (1)$$

where V_m (mL) is the volume of solution in the meniscus, t (min) is the time, and ρ_p (g cm^{-3}) is the density of the polymer film, which we assume to be constant and equal to 1.1 g cm^{-3}, due to experimental difficulties with the measurement of this quantity for polymer thin films. The prefactors in eq 1 allowed us to directly input variables with the units listed in Table 1. Applying eq 1 to the previously described process characterization experiments allows for the approximate quantitative characterization of the accumulation of polymer solution in the meniscus during the runs, a posteriori (see Table S6). In general, this analysis showed that the process could reliably produce uniform films under steady state conditions or in a state of accumulation.

Table 1. Process Variables and Materials Properties[a]

parameter	variable	range of values	units
film thickness	H	10–100	nm
width of trough	w	10	cm
velocity	v	2–6	mm s^{-1}
solution pump rate	Q	20–100	μL min^{-1}
solution concentration	C	5–40	mg mL^{-1}
polymer density (solid)	ρ_p	1.1	g cm^{-3}
polymer solution viscosity	μ_s	1–10	MPa s
polymer solution density	ρ_s	1.1–1.5	g cm^{-3}
evaporative mass transfer coefficient	K_{evap}	7.75×10^{-6}	cm s^{-1}
spreading coefficient	S	−4.2–12.1	

[a]Spreading coefficients were calculated from interfacial surface tensions (Tables S2 and S3).

3.1.6. Process Design Strategy. The process characterization experiments show that, in lieu of a predictive transport model describing the physics of the process, an iterative empirical approach can be applied to design a reliable process operating at or near steady-state conditions. To coat a given polymer solution to a desired thickness, the following strategy can be applied: (i) characterize the range of thicknesses accessible via modulation of the concentration of the polymer solution, (ii) choose the concentration that will yield the desired thickness, (iii) find the maximum drawing velocity for the chosen concentration, and (iv) apply eq 1 to solve for the solution pump rate that will yield approximately steady-state conditions. If the process is designed appropriately, it can be used to coat a film of consistent and desired thickness for a long duration of time. Since our benchtop setup was limited to a 0.5 m loop of PET, we demonstrated this consistency by measuring the thickness of the film after each incremental layer was added. As can be seen in Figure 4, by choosing the correct steady-state operating conditions, we were able to produce a film of consistent and desired thickness, over a timescale of >15 min. Further studies into the effects of surface tension, viscosity, and mass transfer coefficient of the polymer solution on the characteristic thickness of the polymer film could yield a

DOI: 10.1021/acs.chemmater.9b03343
Chem. Mater. XXXX, XXX, XXX–XXX

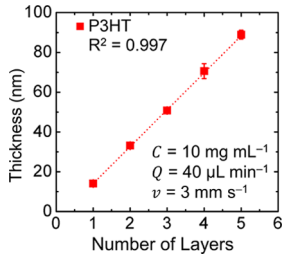

Figure 4. Consistency of film thickness over time. Each successive layer of P3HT is of the same thickness, over a length of 50 cm between each layer, showing that the process is operating under steady-state conditions.

deeper understanding of the physical processes underlying the spreading and drying phenomena. Such knowledge could help develop a theoretical model to predict the final film thickness a priori.

3.1.7. Termination of Process. In all cases, the solid floating polymer films would eventually tear on the surface of the water bath or lose cohesion with the bilayer meniscus (see Movie S2). Both of these modes of failure were initiated by vibrations, airflow, or other external disruptions from the laboratory that could, in principle, be mitigated by further isolating the apparatus and improving the construction. After the film fractured, it was initially difficult to regenerate a solid film, as the injected polymer solution accumulated only along the PTFE walls of the water bath, rather than continuing to spread. We found that the water bath had a higher contact angle on the PTFE once the solution stopped spreading (115° vs 109° for DI water, see Figures S4e,f and S5 and Table S7), indicating that the surface energy between the water and air had decreased. Given that the spreading coefficient of chlorobenzene is already close to zero (Table S3), such a small change in surface energy could easily cause the spreading parameter of the polymer solution to shift from positive to negative; the reduced surface energy therefore inhibits subsequent spreading. Thus, while physical disruptions such as vibrations were responsible for causing the spreading of the polymer solution to cease, chemical contamination of the water bath prevented the subsequent restart of the process. However, after several more minutes, the spreading process would often restart spontaneously, likely due to surface contamination becoming dissipated into the water bath bulk. Working with higher purity starting materials—or finding a way to continually replenish the water bath—could likely improve the long-term stability of the system.

3.2. Mechanical Properties of Films from Interfacial Drawing. *3.2.1. Elastic Modulus.* Our laboratory has a specific interest in the mechanical properties of semiconducting polymers for robust and stretchable devices for energy and healthcare.[37] The elastic moduli and fracture strain of P3HT, PTB7, and J51:N2200 were measured using a film-on-water uniaxial tensile test. Representative stress−strain curves are given in Figure S6. Figure 5a compares the moduli of films of these three materials prepared by spin-coating and interfacial drawing. All three of our materials exhibited a lower elastic modulus when prepared via interfacial drawing versus spin-coating. We attribute this improved compliance to the more rapid rate of drying in interfacial drawing, which occurs over a timescale of seconds, compared to several minutes for spin-coating.[22] Previous modeling work by our group and others has suggested that a faster rate of solidification results in an

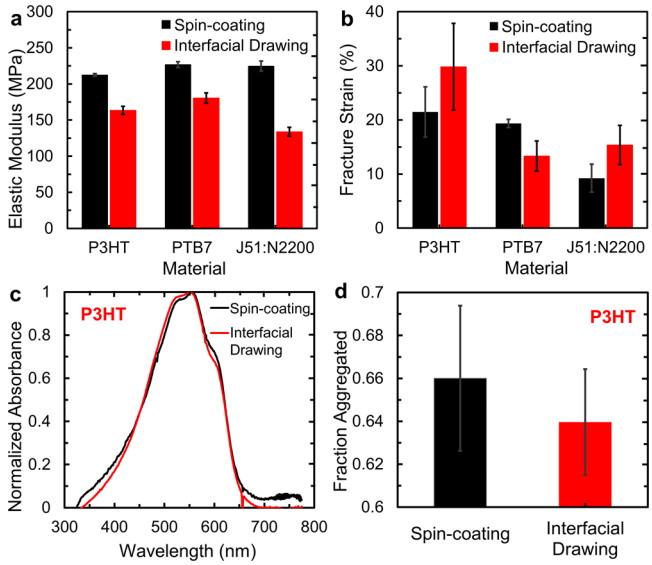

Figure 5. Mechanical properties of films generated from interfacial drawing and spin-coating, comparing (a) elastic modulus and (b) fracture strain for P3HT, PTB7, and J51:N2200. (c) Absorbance vs wavelength UV−vis spectra (normalized to the 0−1 transition at 551 nm), and (d) H-aggregate analysis for representative P3HT samples prepared by spin-coating and interfacial drawing.

increase in void space within the polymer film, and thus a decrease in modulus.[44,45] In many cases, it is desirable to affect the mechanical properties of materials by a way of processing, as opposed to by making changes to the molecular weight or the chemical structure. For example, decreased elastic modulus can be desirable for applications in wearable "epidermal electronics", as the modulus of the device can more closely match the modulus of skin and thus be "invisible" to the user.[46]

3.2.2. Extensibility. A high extensibility is desirable for flexible or stretchable devices. As shown in Figure 5b, P3HT and J51:N2200 exhibited an increased strain at fracture when prepared by spin-coating, whereas for PTB7, the extensibility was reduced. We attribute these findings to the semicrystalline nature of P3HT,[47] J51,[42] and N2200,[41] in contrast to the predominantly amorphous structure of PTB7.[39] The rapid drying rate in interfacial drawing results in a decrease in aggregation in semicrystalline films compared to spin-coating, which, in turn, allows for greater extensibility.[45] This observation is supported by the UV−vis spectra and H-aggregate analysis[48] of our P3HT films (Figure 5c,d). In films from interfacial drawing, the 0−0 transition at 606 nm is reduced, while there is an increase in the region associated with absorption of the amorphous fraction between 450 and 500 nm, indicating decreased aggregated fraction.[49] In contrast, since PTB7 has few ordered domains to begin with, we surmise that the rapid drying rate found in interfacial drawing does not produce the same effect. Instead, the amorphous chains have less time to form entanglements, resulting in decreased extensibility compared to spin-coating.[44]

3.3. Coating Polymer Films onto Textile Substrates. Solution processing of polymer films onto porous, uneven, or textile substrates is inherently challenging due to uneven film morphology that results upon solidification of films. Figure 6a shows the effect of spin-coating a polymer film onto a fabric substrate. As the polymer solution permeates into the weave of the material, individual fibers become coated with the desired

DOI: 10.1021/acs.chemmater.9b03343
Chem. Mater. XXXX, XXX, XXX−XXX

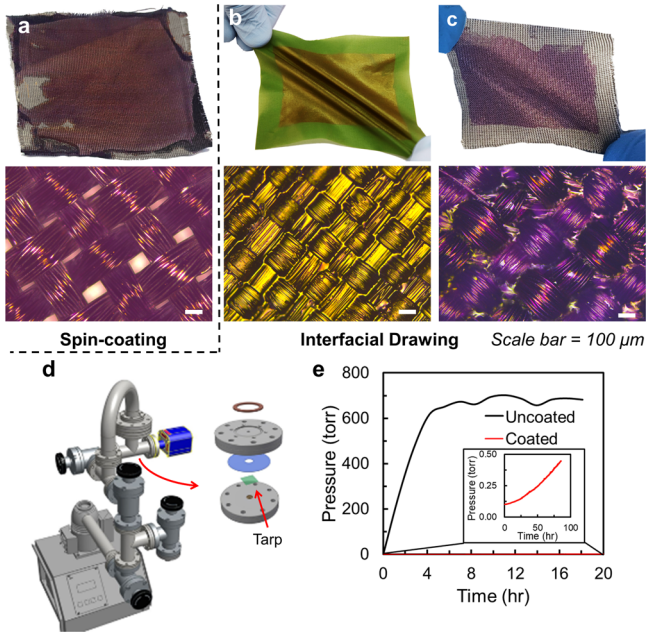

Figure 6. Interfacial drawing with textile substrates. (a) Spin-coating J51:N2200 onto silver nylon tarp. (b) A single layer of P3HT (~40 nm) coated onto Ripstop silnylon tarp, and (c) J51:N2200 (~30 nm) coated onto silver nylon tarp, using interfacial drawing. (d) Schematic of isochoric gas permeability apparatus, used to measure air permeability of fabrics and barrier films. (e) Pressure vs time plots for uncoated Ripstop silnylon tarp and tarp coated with PMMA via interfacial drawing.

polymer, leaving gaps between fiber bundles. For some applications, this uneven morphology may be preferred, such as in the fabrication of conductive fabrics for heating applications.[32,50] In other cases, such as the application of a polymer film to a porous substrate to reduce its permeability in a controlled manner, it is desirable to adhere a cohesive polymer film with a uniform thickness. Figure 6b,c shows how polymer films can be coated onto (rather than absorbed into) the surface of a fabric using interfacial drawing. This method was successful with fabrics with a narrow spacing, such as "Ripstop" silnylon fabric (Figure 6b) as well as those with a wide spacing between fibers, such as a silver-coated conductive nylon textile (Figure 6c). The brightly colored materials shown in Figure 6a–c were chosen to aid visualization of the resultant polymer film structure when using textile substrates with interfacial drawing. PMMA is better suited for coating a fabric to render it impermeable to air or water. We coated two layers of PMMA onto a piece of a Ripstop silnylon tarp and measured its permeability to air using a custom-designed isochoric gas permeability apparatus, as shown in Figure 6d. After the system is placed under a static vacuum of <0.1 torr, one side is exposed to atmospheric pressure, causing the pressure on the vacuum side to slowly increase. As shown in Figure 6e, the PMMA acted as a barrier, reducing gas permeability by four orders of magnitude.

3.4. Flexible Organic Solar Cells. To demonstrate the capability of interfacial drawing for producing functioning organic electronic devices, we fabricated flexible organic solar cells using indium-doped tin oxide (ITO)/PET substrates and an active layer of J51:N2200. Achieving an optimal active layer thickness of 120 nm, as reported by Gao et al.,[42] required coating the substrates with four successive layers of 30 nm-thick polymer films. A representative $J-V$ plot for our solar cells, as well as for control devices fabricated via spin-coating, is shown in Figure 7, with tabulated solar cell performance

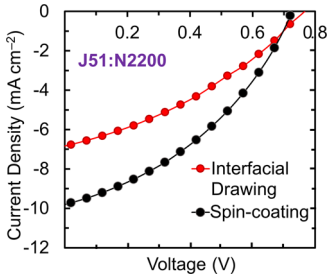

Figure 7. Flexible organic solar cells. Representative current density–voltage plots for solar cells fabricated using interfacial drawing and spin-coating. The full device architecture was PET/ITO/PEDOT:PSS (10 nm)/J51:N2200 (120 nm)/EGaIn.

metrics given in Table 2. While the previous work on fabricating organic solar cells from solution-spread (non-R2R) polymer thin films reported an improved power conversion efficiency compared to spin-coating,[22] we observed a decrease in efficiency from 2.54 to 1.71%. This difference is a result of a decrease in current density in our devices produced by interfacial drawing along with a small decrease in fill factor. We attribute this reduced performance to interruption in charge transport between discrete layers of J51:N2200 films and possible contamination by water. We attempted to increase the cohesion between successively deposited layers by thermal annealing; however, this action caused the efficiency to further decrease, likely due to unfavorable phase separation between the donor and acceptor material. We note that these solar cells were otherwise unoptimized. We included the result as an example of the ability of interfacial drawing to generate functional semiconducting devices, despite conventional wisdom that suggests that semiconducting polymers are easily degraded by oxygen and water.[51,52] We nevertheless believe that further optimization could substantially increase the efficiency of solar cells produced via interfacial drawing. Further investigations into a wider array of donor and acceptor materials would likely reveal a materials system, which is better suited for high-efficiency flexible devices and will be the area of focus for future studies by our group.

4. CONCLUSIONS

We introduced a new R2R process—interfacial drawing—for coating arbitrary substrates with solid polymer thin films supported by the surface tension of water. Experimental results show that the film thickness can be precisely controlled in a range of 10–80 nm by empirical tuning the concentration of the polymer solution as well as the drawing velocity and input flowrate of the polymer solution. We determined that, in comparison to spin-coated films, interfacial drawing yields films with a reduced elastic modulus and an increased extensibility (for semicrystalline materials), which are often desirable mechanical properties for stretchable and flexible devices. Finally, we demonstrated the utility of interfacial drawing by successfully fabricating flexible organic solar cells and by coating polymer films onto textiles for use as fabric-mounted devices and barriers. Future optimization of interfacial drawing will involve developing a detailed theoretical model of the transport process to circumvent the empirical strategy

DOI: 10.1021/acs.chemmater.9b03343
Chem. Mater. XXXX, XXX, XXX–XXX

Table 2. Performance Metrics for Flexible J51:N2200 Organic Solar Cells on ITO/PET Substrates, Comparing Devices Prepared by Interfacial Drawing and by Spin-Coating[a]

method	V_{oc} (V)	J_{sc} (mA cm^{-2})	FF	PCE (%)
spin-coating	0.68 ± 0.05 (0.72)	10.04 ± 0.42 (10.55)	0.38 ± 0.01 (0.39)	2.54 ± 0.18 (2.75)
interfacial drawing	0.78 ± 0.01 (0.79)	6.31 ± 0.55 (6.83)	0.35 ± 0.01 (0.36)	1.71 ± 0.15 (1.81)

[a]Average and standard deviations are given for n = 5 devices, with champion values given in parentheses.

currently employed for designing the process. Furthermore, improved isolation of the apparatus from external vibrations, as well as scaling up the process to a larger water bath, should allow for the faster coating of more uniform films over larger areas. This process should be of interest to organic materials of chemists aiming to develop novel architectures of biosensors, solar cells, and wearable electronics, as well as engineers seeking new roll-to-roll processing techniques for fabricating large-area polymer thin films.

5. MATERIALS AND METHODS

5.1. Materials. Poly(3-hexylthiophene) (P3HT; M_n = 85−100 kDa) and poly(methyl methacrylate) (PMMA; Mn = 400−550, kDa) were obtained from Sigma-Aldrich. Poly[[4,8-bis[(2-ethylhexyl)oxy]-benzo[1,2-*b*:4,5-*b*′]dithiophene-2,6-diyl][3-fluoro-2-[(2-ethylhexyl) carbonyl]thieno [3,4-b]thiophenediyl]] (PTB7; M_n = 80−100 kDa), poly[(5,6-difluoro-2-octyl-2*H*-benzotriazole-4,7-diyl)-2,5-thiophenediyl[4,8-bis[5-(2-hexyldecyl)-2-thienyl]benzo[1,2-*b*:4,5-*b*′]-dithiophene-2,6-diyl]-2,5-thiophenediyl] (J51; M_n = 40 kDa, PDI = 2.6), and poly[[1,2,3,6,7,8-hexahydro-2,7-bis(2-octyldodecyl)-1,3,6,8-dioxobenzo[*lmn*][3,8]phenanthroline-4,9-diyl][3,3′-bisfluoro-2,2′-bithiophene]- 5,5′-diyl] (N2200; M_n = 200 kDa, PDI = 2−3) were obtained from ONE Material. PEDOT:PSS (Clevios PH1000) was purchased from Heraeus. ITO-coated PET was purchased from Adafruit and had a sheet resistance of <60 Ω □$^{-1}$. Chlorobenzene, acetone, isopropanol, and 1,8-diiodooctane (DIO) were obtained from Sigma-Aldrich and were used as received. Adhesive-coated poly(tetrafluoroethylene) (PTFE) was purchased from 3M. Flexible poly(ethylene terephthalate) (PET) was obtained from infinityPV, while silnylon Ripstop tarp and silver-coated nylon fabric were purchased from Assurance Fabrics.

5.2. Interfacial Drawing Operation. Between trials, the trough was cleaned with water, acetone, and isopropanol and dried thoroughly. To begin a trial, the trough was placed under the bottom roller and filled with DI water. The polymer solution was transferred to a 1 mL syringe, which was connected to PTFE tubing that was clamped to the water bath edge. The entire setup was placed under a fume snorkel to eliminate solvent fumes. The flow rate of the polymer solution was controlled with a syringe pump, which we varied from 10 to 100 μL min^{-1}. Once a dry film of the polymer had formed on the water bath, the rollers were set in motion and the polymer film was drawn by the rolling film of PET. Trials were run over a range of 2−7 mm s^{-1}. Other substrates, such as nylon fabrics and ITO-coated PET, could easily be cut and adhered to the PET loop using a double-sided tape.

5.3. Thickness Analysis. *5.3.1. Thickness Calibration.* The ease of gathering UV−vis spectra allowed us to map thickness variations across large-area films and to efficiently measure the thickness of many films. We did this by correlating peak absorption to film thickness for P3HT, PTB7, and J51:N2200 and then estimating the thickness of our unknown samples based on their UV−vis spectra. To generate these correlations, we prepared solutions of each material in chlorobenzene, which were stirred overnight and then filtered through a 1 μm PTFE filter. Glass slides measuring 2.5 × 2.5 cm^2 were sonicated sequentially for 10 min in detergent, DI water, acetone, and isopropanol and then dried and treated with plasma (30 W) for 5 min at a base pressure of 250 mTorr of air. We spin-coated six to eight samples for each curve using concentrations ranging from 5 to 20 mg mL^{-1} and spin speeds ranging from 500 to 2000 rpm. Samples were then cut into 1 cm^2 pieces, and absorbance was measured using UV−vis (Agilent) over a range of 300−900 nm. Our samples ranged in peak absorbance from 0.1 to 1.2 AU. Next, we scratched a notch through the surface of each film to provide a step height for thickness measurements. Thickness was measured with a Veeco atomic force microscope (AFM) in a noncontact tapping mode and analyzed using Nanoscope software. Our samples ranged in thickness from 10 to 200 nm. We found a very accurate fit between peak absorbance and thickness (R^2 > 0.98 for all materials) and did not extrapolate thicknesses beyond the range of our calibration curves. These correlations are found in the Supporting Information (Figure S7).

5.3.2. Roll-to-Roll Thickness Analysis. We studied the effect of various parameters on the final thin film thickness by varying process variables (defined in Table 1) individually. Absorbances were measured by UV−vis and converted to thickness as described above. We did observe some spatial variation in film thicknesses along the edges of the films, so we made sure to test the middle region of our films in at least five locations to obtain an average thickness for each trial.

5.4. Mechanical Properties of Polymer Thin Films. The mechanical properties of our polymer films were determined using film-on-water (FOW) uniaxial tensile tests, originally developed by Kim et al.[53] and reported previously by our group as well.[54] Detailed instructions are available in the Supporting Information (Figure S6). Briefly, polymer films were deposited onto glass slides coated with a water-soluble layer of PEDOT:PSS. The slides were lowered into a water bath, causing the PEDOT:PSS to dissolve. The resulting free-standing polymer films were adhered to grips, which are attached to a linear actuator. A load cell connected to the linear actuator recorded applied force versus displacement, which was then converted to stress versus strain using the dimensions of the polymer film and the initial elongation. The elastic modulus was estimated as the slope of the linear regime of the stress−strain curve. The fracture strain was reported as the strain at failure.

5.5. Polymer Films on Porous and Textile Substrates. Pieces of the silnylon Ripstop tarp and silver-coated nylon tarp were cut into squares. Spin-coated samples were placed on a large glass slide, and the polymer solution was applied via dynamic spin-coating at 1000 rpm. For samples prepared via interfacial drawing, the fabric squares were adhered to the PET loop using tape. Samples were imaged under a Leica optical microscope. Our PMMA-coated samples were placed within an isochoric gas permeability apparatus, in which the entire system was placed under a static vacuum (<0.1 torr), after which one side was subsequently exposed to atmospheric pressure. The area through which the gas could permeate was 0.2 cm^2. A vacuum gauge measured the change in pressure over time in the downstream chamber, with a volume of 25 cm^3.

5.6. Flexible Organic Solar Cells. *5.6.1. Device Fabrication.* A solution of N2200 (8 mg mL^{-1}) and J51 (4 mg mL^{-1}) in chlorobenzene with 1% by volume 1,8-diiodooctane (DIO) was prepared and stirred overnight. Our flexible bottom electrode was ITO/PET, which was cut into 2.5 cm × 2 cm pieces, and sequentially sonicated for 10 min in detergent, DI water, acetone, and isopropanol. The ITO/PET was then dried and treated with plasma (30 W) for 5 min at a base pressure of 250 mTorr of air. Next, a thin layer (10 nm) of PEDOT:PSS was applied via spin-coating according to previously reported methods at 2000 rpm for 60 s.[42] The substrates were annealed on a hot plate in air at 150 °C for 20 min and then allowed to cool. We affixed the PEDOT-coated substrates to the roll-to-roll apparatus with a double-sided tape. We used a pumping rate of 40 μL min^{-1} and a velocity of 3 mm s^{-1}, which resulted in a thickness of 30 nm. Thus, we coated four layers of J51:N2200 to get a comparable

DOI: 10.1021/acs.chemmater.9b03343
Chem. Mater. XXXX, XXX, XXX−XXX

120 nm-thick active layer. We also prepared control devices by spin-coating the active layer onto the substrates. For these control devices, we spin-coated the J51:N2200 solution at 900 rpm for 90 s, followed by 2000 rpm for 30 s, to afford a thickness of 120 nm. All devices were then placed into a glovebox for measurement and allowed to sit under vacuum in the antechamber for 5 min to reduce the amount of adsorbed water on the surface. Device efficiency was measured using a eutectic indium−gallium (EGaIn) top contact.

5.6.2. Measurement of Flexible Solar Cells. The current density versus voltage ($J-V$) characteristics of the cells were measured from −0.2 to 1.0 V using an ABET Sun 2000 solar simulator under an irradiance of 100 mW cm^{-2} from a 150 W Xe short-arc lamp filtered by an AM 1.5G filter. Spectral intensity was calibrated with a Si reference cell. The voltage scan rate was 10 mV s^{-1}. The active area of the devices was determined by the size of the EGaIn drop placed on the surface, which was measured for each trial using a digital camera.

■ ASSOCIATED CONTENT

Supporting Information

The Supporting Information is available free of charge on the ACS Publications website at DOI: 10.1021/acs.chemmater.9b03343.

Annotated photograph of benchtop apparatus for interfacial drawing, contact angle and surface tension measurements, spreading parameters, evaporative mass transfer coefficients, viscosity measurements, photographs of successful and failed trials, summary of process operation parameters, effect of water bath contamination, representative stress−strain curves for materials tested, thickness vs max absorbance (via UV−vis) correlations for materials tested, SEM and AFM images of samples, H-aggregate analysis of P3HT films, and descriptions of videos (PDF)

Video showing termination of trial (MP4)

Video showing startup and steady-state operation (MP4)

■ AUTHOR INFORMATION

Corresponding Author

*E-mail: dlipomi@eng.ucsd.edu.

ORCID

Darren J. Lipomi: 0000-0002-5808-7765

Author Contributions

†R.R. and S.E.R. contributed equally.

Notes

The authors declare no competing financial interest.

■ ACKNOWLEDGMENTS

This work was supported by the Air Force Office of Scientific Research (AFOSR) grant no. FA9550-19-1-0278 and a gift from the B Quest Giving Fund made to D.J.L. through Benefunder. Further support was provided by a gift from Corning in support of the work of S.E.R. Additionally, R.R. received support from the National Science Foundation Graduate Research Fellowship under grant no. DGE-1144086. The authors also thank Andrew Kleinschmidt, Mohammad A. Alkhadra, Prof. Laure V. Kayser, and Dr. Cody Carpenter for helpful discussion.

■ REFERENCES

(1) Yim, K.-H.; Zheng, Z.; Liang, Z.; Friend, R. H.; Huck, W. T. S.; Kim, J.-S. Efficient Conjugated-Polymer Optoelectronic Devices Fabricated by Thin-Film Transfer-Printing Technique. *Adv. Funct. Mater.* **2008**, *18*, 1012−1019.

(2) Tada, A.; Geng, Y.; Wei, Q.; Hashimoto, K.; Tajima, K. Tailoring Organic heterojunction interfaces in bilayer Polymer Photovoltaic Devices. *Nat. Mater.* **2011**, *10*, 450−455.

(3) O'Connor, T. F.; Zaretski, A. V.; Shiravi, B. A.; Savagatrup, S.; Printz, A. D.; Diaz, M. I.; Lipomi, D. J. Stretching and Conformal Bonding of Organic Solar Cells to Hemispherical Surfaces. *Energy Environ. Sci.* **2014**, *7*, 370−378.

(4) Peumans, P.; Forrest, S. R. Very-High-Efficiency Double-Heterostructure Copper Phthalocyanine/C60 Photovoltaic Cells. *Appl. Phys. Lett.* **2001**, *79*, 126−128.

(5) Cnops, K.; Zango, G.; Genoe, J.; Heremans, P.; Martinez-Diaz, M. V.; Torres, T.; Cheyns, D. Energy Level Tuning of Non-Fullerene Acceptors in Organic Solar Cells. *J. Am. Chem. Soc.* **2015**, *137*, 8991−8997.

(6) Aguirre, J. C.; Hawks, S. A.; Ferreira, A. S.; Yee, P.; Subramaniyan, S.; Jenekhe, S. A.; Tolbert, S. H.; Schwartz, B. J. Sequential Processing for Organic Photovoltaics : Design Rules for Morphology Control by Tailored Semi-Orthogonal Solvent Blends. *Adv. Energy Mater.* **2015**, *5*, 1−11.

(7) Ye, L.; Xiong, Y.; Chen, Z.; Zhang, Q.; Fei, Z.; Henry, R.; Heeney, M.; O'Connor, B. T.; You, W.; Ade, H. Sequential Deposition of Organic Films with Eco-Compatible Solvents Improves Performance and Enables Over 12%-Efficiency Nonfullerene Solar Cells. *Adv. Mater.* **2019**, *31*, 1808153.

(8) Søndergaard, R. R.; Hösel, M.; Krebs, F. C. Roll-to-Roll Fabrication of Large Area Functional Organic Materials. *J. Polym. Sci., Part B: Polym. Phys.* **2013**, *51*, 16−34.

(9) Behroozi, P.; Cordray, K.; Griffin, W.; Behroozi, F. The Calming Effect of Oil on Water. *Am. J. Phys.* **2007**, *75*, 407−414.

(10) Rayleigh, L. Measurements of the Amount of Oil Necessary in Order to Check the Motions of Camphor upon Water. *Proc. R. Soc. London* **1889**, *47*, 364−367.

(11) Large, M. J.; Ogilvie, S. P.; King, A. A. K.; Dalton, A. B. Understanding Solvent Spreading for Langmuir Deposition of Nanomaterial Films: A Hansen Solubility Parameter Approach. *Langmuir* **2017**, *33*, 14766−14771.

(12) Roberts, G. G. An Applied Science Perspective of Langmuir-Blodgett Films. *Adv. Phys.* **1985**, *34*, 475−512.

(13) Hickel, W.; Duda, G.; Jurich, M.; Kroehl, T.; Rochford, K.; Stegeman, G. I.; Swalen, J. D.; Wegner, G.; Knoll, W. Optical Waveguides from Novel Polymeric Langmuir-Blodgett Multilayer Assemblies. *Langmuir* **1990**, *6*, 1403−1407.

(14) Östergård, T.; Paloheimo, J.; Pal, A. J.; Stubb, H. Langmuir-Blodgett Light-Emitting Diodes of Poly (3-Hexylthiophene) : Electro-Optical Characteristics Related to Structure. *Synth. Met.* **1997**, *88*, 171−177.

(15) Correia, F. C.; Wang, S. H.; Péres, L. O.; Caseli, L. Langmuir and Langmuir−Blodgett films of a Quinoline-Fluorene Based Copolymer. *Colloids Surf., A* **2012**, *394*, 67−73.

(16) Inukai, K.; Hotta, Y.; Tomura, S.; Takahashi, M.; Yamagishi, A. Preparation of the Langmuir - Blodgett Film of a Clay - Alkylammonium Adduct and Its Use as a Barrier for Interlayer Photoinduced Electron Transfer. *Langmuir* **2000**, *16*, 7679−7684.

(17) Petty, M. C. Possible Applications for Langmuir-Blodgett Films. *Thin Solid Films* **1992**, *210-211*, 417−426.

(18) Demond, A. H.; Lindner, A. S. Estimation of Interfacial Tension between Organic Liquids and Water. *Environ. Sci. Technol.* **1993**, *27*, 2318−2331.

(19) Morita, T.; Singh, V.; Nagamatsu, S.; Oku, S.; Takashima, W.; Kaneto, K. Enhancement of Transport Characteristics in Poly(3-Hexylthiophene) Films Deposited with Floating Film Transfer Method. *Appl. Phys. Express* **2009**, *2*, 111502.

(20) Kawaguchi, M.; Tohyama, M.; Mutoh, Y.; Takahashi, A. Ellipsometric Study of Polymer Monolayers Spread at the Air-Water Interface. 1. Thickness of Monolayers. *Langmuir* **1988**, *4*, 407−410.

DOI: 10.1021/acs.chemmater.9b03343
Chem. Mater. XXXX, XXX, XXX−XXX

(21) Kumaki, J. Polystyrene Monomolecular Particles Obtained by Spreading Dilute Solutions on the Water Surface. *Macromolecules* **1986**, *19*, 2258−2263.
(22) Noh, J.; Jeong, S.; Lee, J.-Y. Ultrafast Formation of Air-Processable and High-Quality Polymer Films on an Aqueous Substrate. *Nat. Commun.* **2016**, *7*, 12374.
(23) Forester, R. H.; Francis, P. S. Method of Producing an Ultrathin Polymer Film Laminate. U.S. Patent 3,551,244, 1970.
(24) Mockus, L.; Reklaitis, G. V. Continuous Time Representation Approach to Batch and Continuous Process Scheduling. 1. MINLP Formulation. *Ind. Eng. Chem. Res.* **1999**, *38*, 197−203.
(25) Kumar, B.; Kaushik, B. K.; Negi, Y. S. Organic Thin Film Transistors: Structures, Models, Materials, Fabrication, and Applications: A Review. *Polym. Rev.* **2014**, *54*, 33−111.
(26) Gevaerts, V. S.; Koster, L. J. A.; Wienk, M. M.; Janssen, R. A. J. Discriminating between Bilayer and Bulk Heterojunction Polymer : Fullerene Solar Cells Using the External Quantum Efficiency. *ACS Appl. Mater. Interfaces* **2011**, *3*, 3252−3255.
(27) Gilbert, L. R.; Weber, M. F.; Strharsky, R. J.; Stover, C. A.; Nevitt, T. J.; Ouderkirk, A. J. Giant Birefringent Optics in Multilayer Polymer Filters. *Opt. Interference Coat.* **2001**, FA2.
(28) Son, D.; Lee, J.; Qiao, S.; Ghaffari, R.; Kim, J.; Lee, J. E.; Song, C.; Kim, S. J.; Lee, D. J.; Jun, S. W.; et al. Multifunctional Wearable Devices for Diagnosis and Therapy of Movement Disorders. *Nat. Nanotechnol.* **2014**, *9*, 397−404.
(29) Moraes, M. R.; Alves, A. C.; Toptan, F.; Martins, M. S.; Vieira, E. M. F.; Paleo, A. J.; Souto, A. P.; Santos, W. L. F.; Esteves, M. F.; Zille, A. Glycerol / PEDOT : PSS Coated Woven Fabric as a Flexible Heating Element on Textiles. *J. Mater. Chem. C* **2017**, *5*, 3807−3822.
(30) Cohen David, N.; David, Y.; Katz, N.; Milanovich, M.; Anavi, D.; Buzhor, M.; Amir, E. Electro-Conductive Fabrics Based on Dip Coating of Cotton in Poly (3-Hexylthiophene). *Polym. Adv. Technol.* **2017**, *28*, 583−589.
(31) Bashir, T.; Skrifvars, M.; Persson, N.-K. Production of Highly Conductive Textile Viscose Yarns by Chemical Vapor Deposition Technique : A Route to Continuous Process. *Polym. Adv. Technol.* **2011**, *22*, 2214−2221.
(32) Zhang, L.; Baima, M.; Andrew, T. L. Transforming Commercial Textiles and Threads into Sewable and Weavable Electric Heaters. *ACS Appl. Mater. Interfaces* **2017**, *9*, 32299−32307.
(33) Jahan Biglari, M.; Mokhtari, J.; Nouri, M.; Sarabi, A. A. Chemical Vapor Deposition of Poly (3-Alkylthiophene) Nanoparticles on Fabric : Chemical and Electrochemical Characterization. *J. Appl. Polym. Sci.* **2014**, *131*, 40673.
(34) Krebs, F. C. Fabrication and Processing of Polymer Solar Cells: A Review of Printing and Coating Techniques. *Sol. Energy Mater. Sol. Cells* **2009**, *93*, 394−412.
(35) O'Connor, B.; Pipe, K. P.; Shtein, M. Fiber Based Organic Photovoltaic Devices. *Appl. Phys. Lett.* **2008**, *92*, 193306.
(36) Jinno, H.; Fukuda, K.; Xu, X.; Park, S.; Suzuki, Y.; Koizumi, M.; Yokota, T.; Osaka, I.; Takimiya, K.; Someya, T. Stretchable and Waterproof Elastomer-Coated Organic Photovoltaics for Washable Electronic Textile Applications. *Nat. Energy* **2017**, *2*, 780−785.
(37) Root, S. E.; Savagatrup, S.; Printz, A. D.; Rodriquez, D.; Lipomi, D. J. Mechanical Properties of Organic Semiconductors for Stretchable, Highly Flexible, and Mechanically Robust Electronics. *Chem. Rev.* **2017**, *117*, 6467−6499.
(38) Na, J. Y.; Kang, B.; Sin, D. H.; Cho, K.; Park, Y. D. Understanding Solidification of Polythiophene Thin Films during Spin-Coating: Effects of Spin-Coating Time and Processing Additives. *Sci. Rep.* **2015**, *5*, 13288.
(39) Root, S. E.; Alkhadra, M. A.; Rodriquez, D.; Printz, A. D.; Lipomi, D. J. Measuring the Glass Transition Temperature of Conjugated Polymer Films with Ultraviolet-Visible Spectroscopy. *Chem. Mater.* **2017**, *29*, 2646−2654.
(40) Kleinschmidt, A. T.; Root, S. E.; Lipomi, D. J. Poly(3-Hexylthiophene) (P3HT): Fruit Fly or Outlier in Organic Solar Cell Research? *J. Mater. Chem. A* **2017**, *5*, 11396−11400.
(41) Balar, N.; Rech, J. J.; Henry, R.; Ye, L.; Ade, H.; You, W.; O'Connor, B. T. The Importance of Entanglements in Optimizing the Mechanical and Electrical Performance of All-Polymer Solar Cells. *Chem. Mater.* **2019**, *31*, 5124−5132.
(42) Gao, L.; Zhang, Z.-G.; Xue, L.; Min, J.; Zhang, J.; Wei, Z.; Li, Y. All-Polymer Solar Cells Based on Absorption-Complementary Polymer Donor and Acceptor with High Power Conversion Efficiency of 8.27%. *Adv. Mater.* **2016**, *28*, 1884−1890.
(43) Dang, M. T.; Hirsch, L.; Wantz, G. P3HT:PCBM, Best Seller in Polymer Photovoltaic Research. *Adv. Mater.* **2011**, *23*, 3597−3602.
(44) Root, S. E.; Jackson, N. E.; Savagatrup, S.; Arya, G.; Lipomi, D. J. Modelling the Morphology and Thermomechanical Behaviour of Low-Bandgap Conjugated Polymers and Bulk Heterojunction Films. *Energy Environ. Sci.* **2017**, *10*, 558−569.
(45) Awartani, O.; Lemanski, B. I.; Ro, H. W.; Richter, L. J.; De Longchamp, D. M.; O'Connor, B. T. Correlating Stiffness, Ductility, and Morphology of Polymer:Fullerene Films for Solar Cell Applications. *Adv. Energy Mater.* **2013**, *3*, 399−406.
(46) Kim, D.-H.; Lu, N.; Ma, R.; Kim, Y.-S.; Kim, R.-H.; Wang, S.; Wu, J.; Won, S. M.; Tao, H.; Islam, A.; Yu, K. J.; Kim, T.-i.; Chowdhury, R.; Ying, M.; Xu, L.; Li, M.; Chung, H.-J.; Keum, H.; McCormick, M.; Liu, P.; Zhang, Y.-W.; Omenetto, F. G.; Huang, Y.; Coleman, T.; Rogers, J. A. Epidermal Electronics. *Science* **2011**, *333*, 838−843.
(47) Savagatrup, S.; Printz, A. D.; Rodriquez, D.; Lipomi, D. J. Best of Both Worlds: Conjugated Polymers Exhibiting Good Photovoltaic Behavior and High Tensile Elasticity. *Macromolecules* **2014**, *47*, 1981−1992.
(48) Spano, F. C. The Spectral Signatures of Frenkel Polarons in H- and J-Aggregates. *Acc. Chem. Res.* **2010**, *43*, 429−439.
(49) Böckmann, M.; Schemme, T.; De Jong, D. H.; Denz, C.; Heuer, A.; Doltsinis, N. L. Structure of P3HT Crystals, Thin Films, and Solutions by UV/Vis Spectral Analysis. *Phys. Chem. Chem. Phys.* **2015**, *17*, 28616−28625.
(50) Sparavigna, A. C.; Florio, L.; Avloni, J.; Henn, A. Polypyrrole Coated PET Fabrics for Thermal Applications. *Mater. Sci. Appl.* **2010**, *01*, 253−259.
(51) Wang, Y.; Zhan, X. Layer-by-Layer Processed Organic Solar Cells. *Adv. Energy Mater.* **2016**, *6*, 1600414.
(52) Hintz, H.; Egelhaaf, H.-J.; Lüer, L.; Hauch, J.; Peisert, H.; Chassé, T. Photodegradation of P3HT - A Systematic Study of Environmental Factors. *Chem. Mater.* **2011**, *23*, 145−154.
(53) Kim, J.-H.; Nizami, A.; Hwangbo, Y.; Jang, B.; Lee, H.-J.; Woo, C.-S.; Hyun, S.; Kim, T.-S. Tensile Testing of Ultra-Thin Films on Water Surface. *Nat. Commun.* **2013**, *4*, 2520.
(54) Rodriquez, D.; Kim, J.-H.; Root, S. E.; Fei, Z.; Boufflet, P.; Heeney, M.; Kim, T.-S.; Lipomi, D. J. Comparison of Methods for Determining the Mechanical Properties of Semiconducting Polymer Films for Stretchable Electronics. *ACS Appl. Mater. Interfaces* **2017**, *9*, 8855−8862.

DOI: 10.1021/acs.chemmater.9b03343
Chem. Mater. XXXX, XXX, XXX−XXX